THE JOURNAL OF BIOLOGICAL CHEMISTRY VOL. 283, NO. 45, pp. 30850–30860, November 7, 2008

Osteoclast Inhibitory Lectin, an Immune Cell Product That Is Required for Normal Bone Physiology *in Vivo*[*]

Received for publication, March 5, 2008, and in revised form, September 8, 2008 Published, JBC Papers in Press, September 8, 2008, DOI 10.1074/jbc.M801761200

Vicky Kartsogiannis[‡1], Natalie A. Sims[‡§2], Julian M. W. Quinn[‡§1], Chi Ly[‡], Mirijana Cipetić[‡], Ingrid J. Poulton[‡], Emma C. Walker[‡], Hasnawati Saleh[‡§1], Narelle E. McGregor[‡], Morgan E. Wallace[¶3], Mark J. Smyth[¶4], T. John Martin[‡§], Hong Zhou[‡5], Kong Wah Ng[‖], and Matthew T. Gillespie[‡§6]

From the [‡]St. Vincent's Institute, 9 Princes Street, Fitzroy, Victoria 3065, the [§]Department of Medicine, University of Melbourne, St. Vincent's Hospital, 41 Victoria Parade, Fitzroy, Victoria 3065, [¶]Cancer Immunology Program, Peter MacCallum Cancer Centre, Locked Bag 1, A'Beckett St., 8006 Victoria, and the [‖]Department of Diabetes and Endocrinology, University of Melbourne, St. Vincent's Hospital, 41 Victoria Parade, Fitzroy, Victoria 3065, Australia

Osteoclast inhibitory lectin (OCIL or clrb) is a member of the natural killer cell C-type lectins that have a described role mostly in autoimmune cell function. OCIL was originally identified as an osteoblast-derived inhibitor of osteoclast formation *in vitro*. To determine the physiological function(s) of OCIL, we generated *ocil*$^{-/-}$ mice. These mice appeared healthy and were fertile, with no apparent immune function defect, and phenotypic abnormalities were limited to bone. Histomorphometric analysis revealed a significantly lower tibial trabecular bone volume and trabecular number in the 10- and 16-week-old male *ocil*$^{-/-}$ mice compared with wild type mice. Furthermore, *ocil*$^{-/-}$ mice showed reduced bone formation rate in the 10-week-old females and 16-week-old males while Static markers of bone formation showed no significant changes in male or female *ocil*$^{-/-}$ mice. Examination of bone resorption markers in the long bones of *ocil*$^{-/-}$ mice indicated a transient increase in osteoclast number per unit bone perimeter. Enhanced osteoclast formation was also observed when either bone marrow or splenic cultures were generated *in vitro* from *ocil*$^{-/-}$ mice relative to wild type control cultures. Loss of *ocil* therefore resulted in osteopenia in adult mice primarily as a result of increased osteoclast formation and/or decreased bone formation. The enhanced osteoclastic activity led to elevated serum calcium levels, which resulted in the suppression of circulating parathyroid hormone in 10-week-old *ocil*$^{-/-}$ mice compared with wild type control mice. Collectively, our data suggest that OCIL is a physiological negative regulator of bone.

We have previously identified a family of inhibitors of osteoclast formation that belong to the natural killer (NK)[7] cell receptor group of the C-type lectin superfamily (1–3). Murine osteoclast inhibitory lectin (OCIL, also known as clrb) was the first identified member of this family of type II membrane-bound lectins that includes the related proteins OCILrP1 and OCILrP2/clrg. A human OCIL homologue has also been described (3). The OCIL family share high nucleotide and amino acid sequence identity in the extracellular domain, genomic structure, and biological function, and their hallmark C-type lectin domain shares ~35% identity with CD69. The extracellular domains of the OCIL and OCIL-related proteins, when expressed as recombinant glutathione *S*-transferase fusion proteins, similarly inhibit osteoclast formation in murine bone marrow cultures or spleen cell cultures treated with M-CSF and RANKL (2). Although OCIL/clrb was originally identified in osteoblasts where its expression is regulated by bone-active hormones and cytokines such as parathyroid hormone (PTH), calcitriol, interleukin-1α (IL-1α), IL-11, and retinoic acid, it is also expressed in a number of extraskeletal tissues, particularly epithelial and mesenchymal cell populations and dendritic, macrophage, and lymphocyte populations (1, 4, 5).

Like other C-type lectins, OCIL binds various high molecular weight glycosaminoglycans, including fucoidan, λ-carrageenan, and chondroitin, yet these interactions are not essential for its ability to inhibit osteoclast formation (6). One potential class of receptors for OCIL is the NK cell receptors, which are responsible for major histocompatibility complex class I-independent inhibition of cell killing by NK cells (4, 7). The *ocil/clrb* and *ocilrP2/clrg* genes are located in the NK cell gene complex on the distal portion of mouse chromosome 6 (8, 9). This gene complex also contains numerous genes for other membrane-

* This work was supported by Program Grant 345401 (to M. T. G., T. J. M., N. A. S., and K. W. N.) and Program Grant 454569 (to M. J. S.) from the National Health and Medical Research Council of Australia. The costs of publication of this article were defrayed in part by the payment of page charges. This article must therefore be hereby marked "*advertisement*" in accordance with 18 U.S.C. Section 1734 solely to indicate this fact.

[1] Present address: Prince Henry's Institute, P. O. Box 5152, Clayton, Victoria 3168, Australia.

[2] Senior Research Fellow of the National Health and Medical Research Council of Australia.

[3] Doherty Fellow of the National Health and Medical Research Council of Australia.

[4] Senior Principal Research Fellow of the National Health and Medical Research Council of Australia.

[5] Present address: Anzac Research Institute, University of Sydney, Hospital Road, Concord, New South Wales 2139, Australia.

[6] Principal Research Fellow of the National Health and Medical Research Council of Australia. To whom correspondence should be addressed: Prince Henry's Institute, P. O. Box 5152, Clayton, Victoria 3168, Australia. Tel.: 613-9594-4372; Fax: 613-9594-6125; E-mail: Matthew.Gillespie@princehenrys.org.

[7] The abbreviations used are: NK, natural killer; RANKL, receptor activator of NF-κB ligand; OCIL, osteoclast inhibitory lectin; M-CSF, macrophage colony-stimulating factor; PTH, parathyroid hormone; IL, interleukin; PIPES, 1,4-piperazinediethanesulfonic acid; FITC, fluorescein isothiocyanate; PBS, phosphate-buffered saline; PFA, paraformaldehyde; FBS, fetal bovine serum; 1,25$(OH)_2D_3$, 1,25-dihydroxyvitamin D_3; αMEM, α-minimal essential medium; BFR, bone formation rate; TRAP, tartrate-resistant acid phosphatase; GAPDH, glyceraldehyde-3-phosphate dehydrogenase; RT, reverse transcriptase; ES, embryonic stem; PPARγ, peroxisome proliferator-activated receptor-γ; APC, antigen presenting complex; DIG, digoxigenin; pQCT, peripheral quantitative computed tomography.

bound NK cell-associated C-type lectins, including CD69, CD94, the NKG2 family, Ly49 family, and the Nkrp1 family. The latter includes Nkrp1d and Nkrp1f regulatory receptors, which are expressed by NK cells, and function as receptors for OCIL/clrb and OCILrP2/clrg, respectively (4). Although Nkrp1d-OCIL binding has been reported to play a role in mediating inhibition of NK cell killing of target cells, OCILrP2 has been shown to act as a co-stimulatory molecule for optimal T cell activation (10), implicating the involvement of both proteins in immune recognition. This suggests other roles for OCIL within the bone environment, immune cell function, and possibly in other tissues rich in glycosaminoglycans (cartilage, skin, thymus, intestine, kidney, and connective tissue).

To address the role(s) of OCIL in normal physiology, we generated homozygous *ocil* null ($ocil^{-/-}$) mice and characterized these mice with particular emphasis on their bones and NK cell and leukocyte cell populations to determine the effect of loss of OCIL action on bone metabolism *in vivo*.

EXPERIMENTAL PROCEDURES

Reagents and Cell Culture—Tissue culture flasks, dishes and plates were purchased from Greiner Labortechnik (Frickenhasen, Germany). Recombinant murine GST-RANKL-(158–316) (RANKL) was produced using a bacterial construct kindly provided by Dr. F. Patrick Ross (Washington University School of Medicine, Department of Pathology and Immunology, St. Louis, MO). Human M-CSF was obtained from R & D Systems (Minneapolis, MN). Prostaglandin E_2 was obtained from Sigma, and 1,25-dihydroxyvitamin D_3 ($1,25(OH)_2D_3$) was from Wako Pure Chemical Co. (Osaka, Japan). All other reagents were of analytic grade obtained from standard suppliers.

Cells were cultured in α-minimal essential medium (αMEM) (Invitrogen) containing 10% fetal bovine serum (FBS) (CSL Biosciences, Parkville, Australia). Incubation was carried out at 37 °C in a humidified atmosphere equilibrated with 5% CO_2 in air. The KUSA-O cell line (11), a bi-potential bone marrow stroma-derived cell line previously characterized by Allan *et al.* (12), was used between passages 5 and 20.

Generation of Ocil-null Targeting Vector—The *ocil*-null targeting vector (Fig. 1*A*) was generated by Ozgene Pty. Ltd. (Murdoch, Australia). The homology arms for *ocil* targeting were inserted into a Basic Vector II (pBVII) containing a floxed PGK-neo cassette as well as several unique restriction sites (used in cloning the homology arms). The 5′ arm was designed to begin in intron 1 and finish in intron 2. A cre-mediated deletion of exon III was created in the murine *ocil* gene by insertion of a LoxP site 5′ of exon 2 by PCR approach. This was added in an existing and unique NdeI site. A 511-bp 5′ probe was designed to bind to exon 1 and flanking regions. A 631-bp 3′ probe was designed to bind downstream of exon V. An EcoRV site upstream of the 5′ probe was used in conjunction with the 5′ probe for genomic screening, whereas a second EcoRV site, downstream of the 3′ probe, was similarly used with the 3′ probe for genomic screening. The *ocil* locus also has an EcoRV site 5′ of the targeting region. Additional EcoRV sites inserted in the targeting construct, allowed for the detection of targeted clones. Screening with the 5′ probe revealed an 11.5-kb wild type (WT) band and a 3.3-kb targeted band, whereas screening with the 3′ probe revealed an 11.5-kb WT band and a 4.7-kb targeted band.

The targeting vector was used for homologous recombination by electroporation in Bruce4 (derived from C57BL/6 (13)) embryonic stem (ES) cells. *Ocil*-targeted ES cell clones were identified by PCR and Southern blot hybridization using the 5′- and 3′-flanking probes. The ES cells carrying the correct mutation were injected into BALB/c blastocysts and implanted into foster mothers. Heterozygous WT/floxed mice were generated from the 3′-targeted clone I-4C2 with both the neo and exon 3 flanked by loxP sites. Chimeric progeny were bred with cre-deleter partners, and screening of progeny was performed by Southern blot hybridization of EcoRV-digested genomic tail-tip DNA hybridized with the 5′ probe.

Animals—The *ocil*-null mice used in this study were developed by Ozgene Pty. Ltd. Mice with a heterozygous $ocil^{+/-}$ deletion (of exon 3) were mated to generate experimental $ocil^{-/-}$ mice. The genetic background of these mice was C57BL/6. Heterozygous ($ocil^{+/-}$) mice were maintained on a C57BL/6 background and backcrossed at least five times before bone histomorphometry to get a recombinant inbred strain.

C57BL/6 wild type mice were obtained from the same source, supplied by Animal Resources Centre (Perth, WA, Australia). All animal handling procedures were approved by the animal ethics committee at St. Vincent's Health, Melbourne, Australia.

Serum Biochemistry—PTH levels in mouse serum samples were determined by enzyme-linked immunosorbent assay according to the manufacturer's instructions (Immutopics, Inc.). For the determination of calcium in mouse serum samples, the method described by Leary *et al.* (14) was used. This method employs the use of a single stable reagent, 200 μmol/liter of arsenazo III (Sigma) in 50 mmol/liter PIPES buffer (Sigma) at pH 6.8. $CaCl_2$ (BDH Analar) solution (0–5 mM) was used for the standard curve, and final absorbance was read at 660 nm using a BMG Polarstar Optima plate assay reader.

Flow Cytometric Analysis—For identification of specific leukocyte populations within thymus, spleen, lymph node, liver, or bone marrow, $1–2 \times 10^6$ cells were stained with the following antibodies: for B cells, antigen presenting complex (APC)-conjugated anti-B220, biotinylated anti-IgM (eBiosciences), and FITC-conjugated anti-CD19; for T cells and NKT cells, PE-Cy5.5-conjugated anti-TCR$\alpha\beta$ (eBiosciences), FITC conjugated anti-CD4, APC-conjugated anti-CD8, and PE-conjugated anti-NK1.1; for dendritic cell and other myeloid lineages, FITC-conjugated anti-CD11c, APC-conjugated anti-CD11b, PE-conjugated anti-CD45RA, PE-Cy5.5-conjugated anti-CD8α (eBiosciences), FITC-conjugated anti-Ly6G, and PE-conjugated anti-F4/80. NK cell subsets were further characterized by staining with NK1.1-PE and TCR$\alpha\beta$-PE-Cy5.5 in combination with anti-Ly49C/I-FITC, Ly49G2FITC, Ly49D-FITC, and CD94-biotin. Biotinylated antibodies were visualized by the addition of streptavidin-APC-Cy7. All antibodies were obtained from Pharmingen unless otherwise specified. Data were collected using a FACSDiva flow cytometer (BD Biosciences) and were analyzed using FCS Express software. Dead

cells were excluded on the basis of uptake of the vital dye Fluorogold (Molecular Probes), and 30–50,000 live events were collected for each sample.

Preparation of Cell Suspensions from Primary and Secondary Lymphoid Organs—Bone marrow, thymus, spleen, liver, and lymph nodes were harvested from age-matched C57BL/6 and *ocil*$^{-/-}$ mice. Single cell suspensions of thymus, spleen, and lymph nodes were prepared by gently crushing organs between two frosted glass slides. Bone marrow was isolated from bisected femora by flushing 5 ml of phosphate-buffered saline (PBS), pH 7.0, through the marrow cavity using a syringe attached to a 27-gauge needle. Liver lymphocytes were prepared by first perfusing the liver by injection of 20 ml of saline into the hepatic portal vein and then washing and centrifuging at low speed to remove hepatocytes, before separation over a 37% Percoll gradient.

Dendritic cells (DC) were enriched from the pooled spleens of 2–3 mice following protocols described previously (15). Briefly, spleens were teased apart, and collagenase-digested and separated by centrifugation over a 14.5% Nycodenz density gradient (Sigma). DC-enriched low density spleen cells were collected from the interface and washed twice in Hanks' balanced salt solution/FBS/EDTA before antibody staining for flow cytometry.

RNA Isolation, Reverse Transcriptase (RT)-PCR, and Southern Blot Analysis—Total RNA was isolated from homogenized tails or primary calvarial cells using TRIzol® (Invitrogen) according to the manufacturer's instructions. RNA was treated with RNase-free DNase (Promega, Madison, WI) for 30 min at 37 °C to remove contaminating DNA, followed by re-precipitation. The concentration of the RNA samples was determined by measuring the absorbance at 260 nm, and RNA purity was assessed by the 260/280 nm absorbance ratio. For semi-quantitative RT-PCR, first strand cDNA was synthesized from 1 to 2 μg of total RNA using Superscript III reverse transcriptase (Invitrogen) following random hexamer priming (Invitrogen). cDNA was amplified using the Expand High Fidelity PCR system (Roche Applied Science) and relevant oligonucleotide pairs as described in Table 1. Amplification conditions for PCRs using oligonucleotide pairs for *ocil* (OCILm111 with OCILm81; OCILm114 with OCILm81; OCILm113 with OCILm81) employed a touchdown PCR protocol. Thermal cycling conditions were as follows: 94 °C for 5 min, followed by 12 cycles of 94 °C for 30 s, annealing temperature "step-downs" every 1 cycle of 1 °C (from 72 to 61 °C) for 30 s and 72 °C for 1 min. This was then followed by 28 cycles of 94 °C for 30 s, 60 °C for 30 s, and 72 °C for 1 min. As a normalizing control for semi-quantitative PCR, murine glyceraldehyde-3-phosphate dehydrogenase (GAPDH) was amplified using oligonucleotides GAPDH-4 and GAPDH-5 (Table 1) under the following conditions: 1 cycle at 94 °C for 5 min, followed by 20–25 cycles at 94 °C for 30 s, 58 °C for 30 s, 72 °C for 30 s, and a final extension step of 72 °C for 5–10 min. PCR products were electrophoresed on 1.5% agarose, Southern-blotted, and detected using digoxigenin-labeled oligonucleotide probes (Table 1) based on the DIG oligonucleotide tailing kit specifications (Roche Applied Science). For real time RT-PCR analysis, a total of 5 μg of RNA were reverse-transcribed into cDNA using random primers and Superscript III reverse transcriptase according to the manufacturer's protocol. Quantitative real time PCR was carried out using 200 nM oligonucleotide primers (Table 1) and SYBR®Green 1 (Molecular Probes, Eugene, OR) under the following conditions: 1 cycle at 95 °C for 10 min, followed by 40 cycles of denaturation (95 °C for 30 s), annealing (60 °C for 30 s), extension (72 °C for 30 s), followed by 1 cycle at 95 °C for 1 min, 55 °C for 30 s, and 95 °C for 30 s. Analysis was performed using the Stratagene MxPro-Mx3000P QPCR systems software (Stratagene, CA). The expression levels of all genes used for quantitative real time PCR were normalized against an internal control gene (housekeeping gene, hypoxanthine phosphoribosyltransferase1 (*HPRT1*)).

Tissue Processing for Histology—For histological analysis, various soft tissues and bones were collected from age-matched (newborn to day 1 and 6, 10, and 16 weeks old) and sex-matched *ocil*-null and WT mice and fixed overnight in 4% paraformaldehyde (PFA) in PBS, pH 7.4, at 4 °C. The long bones were decalcified for 10–14 days in 15% EDTA in 0.5% PFA/PBS solution, pH 8.0 (the decalcifying solution was changed daily). All tissues were processed and embedded in paraffin. Five-μm-thick sections were stained with hematoxylin and eosin.

Quantitative Histomorphometry—Tibiae from *ocil*$^{-/-}$ and WT mice were collected at 6, 10, and 16 weeks of age, fixed in 4% PFA in PBS, and embedded in methylmethacrylate (16). Tartrate-resistant acid phosphatase (TRAP) staining was carried out as described previously (17). Bone histomorphometry was carried out according to standardized protocols of the American Society for Bone and Mineral Research (18) using the Osteomeasure system (OsteoMetrics Inc, Decatur, GA). Femoral length and width were determined from contact X-rays using ImageJ 1.36b (19). For assessment of dynamic histomorphometry, mice were injected with calcein twice; 10 and 3 days before tissue collection (16). Quantitative histomorphometry was performed on toluidine blue and xylenol orange-stained undecalcified 5-μm-thick sections of proximal tibiae as described previously (16). Experiments were performed in a blinded fashion. Statistical differences were determined by analysis of variance and Fisher's post hoc test, and $p < 0.05$ was accepted as significant. All values are expressed as means ± S.E.

Peripheral Quantitative Computed Tomography (pQCT) Analysis—Femoral cortical and trabecular bone mineral density, femoral circumference, and femoral cortical thickness were measured by pQCT (Stratec X-CT Research SA+, version 5.5) using methods adapted from Schmidt *et al.* (20). Metaphyseal scans of the distal femur were taken at a resolution of 70 μm; trabecular and cortical measurements (including circumference) were taken at a distance proximal to the distal growth plate of 5 and 25% of the length of the femur, respectively; trabecular bone mineral density was determined as the inner 45% of the total area (peel mode 20). Interassay coefficients of variation were <1%.

Preparation of Primary Calvarial Cells—Primary murine calvarial cell cultures were prepared from neonatal calvariae by sequential collagenase digestion as described previously (21). Briefly, calvariae from newborn pups were excised and washed in PBS. They were then digested in αMEM contain-

TABLE 1

Mouse oligonucleotide primers used for PCR analyses

The following abbreviations are used: BSP, bone sialoprotein; ALP, alkaline phosphatase; C/EBPδ, CCAAT-enhancing binding protein δ; C/EBPα, CCAAT-enhancing binding protein α; PTHR1, parathyroid hormone receptor 1; Bril, bone restricted ifitm-like protein; OPG, osteoprotegerin; HPRT1, hypoxanthine phosphoribosyltransferase 1.

Semi-quantitative PCR oligonucleotides			
OCILm111	Forward	5′-GGCTTCCCTACCTATGCTTAGTC-3′	
OCILm113	Forward	5′-CTCCACTGTGTCTCCTGTTAAA-3′	
OCILm114	Forward	5′-TCTCCAAAGAAATAGTCTCAGAG-3′	
OCILm81	Reverse	5′-TGCTCTGACGACTCTCTGTG-3′	
OCILm115	Detection	5′-CCTCTTGTGCCATGCAGAAG-3′	
GAPDH-4	Forward	5′-CATGGAGAAGGCTGGGGCTC-3′	
GAPDH-5	Reverse	5′-AACGGATACATTGGGGGTAG-3′	
GAPDH-1	Detection	5′-GCTGTGGGCAAGGTCATCCC-3′	
Real time (SYBR® Green) PCR oligonucleotides			**PrimerBank ID**
Adiponectin	Forward	5′-TGTTCCTCTTAATCCTGCCCA-3′	31982351a1
Adiponectin	Reverse	5′-CCAACCTGCACAAGTTCCCTT-3′	31982351a1
ALP	Forward	5′-AAACCCAGACACAAGCATTCC-3′	
ALP	Reverse	5′-TCCACCAGCAAGAAGAAGCC-3′	
BSP	Forward	5′-CCGAAGCCTATGGGACCAC-3′	6680335a3
BSP	Reverse	5′-ATAAGCTCGGTAAGTGTCGCC-3′	6680335a3
C/EBPδ	Forward	5′-CGACTTCAGCGCCTACATTGA-3′	
C/EBPδ	Reverse	5′-CTAGCGACAGACCCCACAC-3′	
C/EBPα	Forward	5′-CAAGAACAGCAACGAGTACCG-3′	
C/EBPα	Reverse	5′-GTCACTGGTCAACTCCAGCAC-3′	
Col1-A1	Forward	5′-CTGGCGGTTCAGGTCCAAT-3′	34328108a3
Col1-A1	Reverse	5′-TTCCAGGCAATCCACGAGC-3′	34328108a3
Bril	Forward	5′-CACCACGAGATCACATGCTCT-3′	33504579a1
Bril	Reverse	5′-GGATGTTGTAGCACTTGGCTT-3′	
HPRT1	Forward	5′-TGATTAGCGATGATGAACCAG-3′	
HPRT1	Reverse	5′-AGAGGGCCACAATGTGATG-3′	
IL-18	Forward	5′-GACTCTTGCGTCAACTTCAAGG-3′	
IL-18	Reverse	5′-CAGGCTGTCTTTTGTCAACGA-3′	
OPG	Forward	5′-TGTCCAGATGGGTTCTTCTCA-3′	31543882a3
OPG	Reverse	5′-CGTTGTCATGTGTTGCATTTCC-3′	31543882a3
Osteocalcin	Forward	5′-AGCAGACACCATGAGGACCATCTT-3′	
Osteocalcin	Reverse	5′-GGACATGAAGGCTTTGTCAGAC-3′	
Osteopontin	Forward	5′-TAGCTTGGCTTATGGACTGAGG-3′	6678113a3
Osteopontin	Reverse	5′-AGACTCACCGCTCTTCATGTG-3′	6678113a3
Osterix	Forward	5′-ATGGCGTCCTCTCTGCTTG-3′	12667798a1
Osterix	Reverse	5′-TGAAAGGTCAGCGTATGGCTT-3′	12667798a1
Ost-ptp	Forward	5′-TGGCAGAATGTCACAATTACC-3′	34328115a3
Ost-ptp	Reverse	5′-CAGAGGCATCGCTCCATGA-3′	
PPARγ	Forward	5′-GGAAAGACAACGGACAAATCAC-3′	
PPARγ	Reverse	5′-TACGGATCGAAACTGGCAC-3′	
PTHR1	Forward	5′-TTCCAGGGATTTTTTGTTGC-3′	
PTHR1	Reverse	5′-AGTCCAATGCCAGTGTCCAG-3′	
RANKL	Forward	5′-TCCAGCTATGATGGAAGGCT-3′	
RANKL	Reverse	5′-GTACCAAGAGGACAGAGTG-3′	
Runx2/cbfa1	Forward	5′-TTCTCCAACCCACGAATGCAC-3′	20806530a3
Runx2/cbfa1	Reverse	5′-CAGGTACGTGTGGTAGTGAGT-3′	20806530a3
Resistin	Forward	5′-AAGAACCTTTCATTTCCCCTCCT-3′	31982423a1
Resistin	Reverse	5′-GTCCAGCAATTTAAGCCAATGTT-3′	31982423a1
TWIST 1	Forward	5′-TCAAGAGGTCTTGCCAATCAGCCA-3′	
TWIST 1	Reverse	5′-ATTTGCAGGCCAGTTTGATCCCAG-3′	
TWIST 2	Forward	5′-GGCCGCCAGGTACATAGAC-3′	6681177a2
TWIST 2	Reverse	5′-GTAGCTGAGACGCTCGTGA-3′	6681177a2

ing 0.1% collagenase type 2 (Worthington, SCIMAR) and dispase (Invitrogen) for 10 min at 37 °C, and the supernatant was discarded. The calvariae were digested four more times with fresh enzymatic solution for 15min each at 37 °C, and the supernatants were pooled and spun down to collect the cells. Cells were then routinely cultured in α-MEM containing 10% FBS for 1 week until confluent and then used for experiments.

Osteoclast Formation Assays—Bone marrow cells were prepared by flushing the marrow cavities of bisected femora and tibiae from adult C57BL/6 and *ocil*$^{-/-}$ mice with PBS. The mouse bone marrow cells were centrifuged, and the pellet was resuspended in α-MEM containing 10% FBS with penicillin and streptomycin. Bone marrow cells were added at 10^5 cells/well to 10-mm diameter plastic tissue culture wells and stimulated with recombinant RANKL (100 ng/ml) and human M-CSF (25 ng/ml). Cells were incubated for 7 days, with one change of medium and mediators at day 3, and then fixed with buffered formaldehyde (4%). Cells were histochemically stained for TRAP as described previously (22). TRAP-positive multinucleated cells (defined as cells with 2 or more nuclei) were counted as osteoclasts. Bone marrow from wild type and *ocil*$^{-/-}$ mice were also co-cultured with KUSA-O cells or primary calvarial cells at 2×10^4 cells/well, in the presence of 10 nM $1,25(OH)_2D_3$ and 100 nM prostaglandin E_2 for 7 days, then fixed, and osteoclast numbers determined. Mouse spleen cells were obtained from adult C57BL/6 or *ocil*$^{-/-}$ male mice and cultured for 7 days in medium containing 10% FBS, M-CSF (25 ng/ml), and soluble RANKL (50 ng/ml).

Statistical Analysis—All values are expressed as means ± S.E. of at least three independent experiments, or in the case of RNA analyses, two independent experiments were performed in

duplicate or triplicate and two independent analyses of RNA levels made. Statistical significance was determined by one- or two-way analysis of variance followed by Fisher's post hoc test using the StatView software package unless otherwise specified. For the analysis of serum PTH levels, a nonparametric statistical test was carried out such as Mann-Whitney followed by post-hoc Fisher's test. $p < 0.05$ was considered statistically significant.

RESULTS

Genotypic Analysis of Ocil$^{-/-}$ Mice—Construction of the *ocil*$^{-/-}$ targeting vector involved the excision of exon 3 of the *ocil* gene. Because of the deletion of this exon, any read-through transcript of OCIL that may arise because of splicing of exons 2–4, or exons 2–5, results in the introduction of a frameshift, and therefore a nonfunctional transcript of OCIL and a resultant inactive protein (Fig. 1*A*). Exon 2 encodes the transmembrane domain of the *ocil* gene, whereas exon 3 encodes the extracellular domain. We previously identified two closely related murine proteins, OCILrP1 and OCILrP2, which have similar osteoclast-inhibitory actions to OCIL (2). Although the related proteins OCILrP1 and OCILrP2 are the products of separate genes, they share high nucleotide sequence identity (~90%) with OCIL, which is confined to exons 2–5 and intervening introns of OCIL with the corresponding regions (exons 3–6) of OCILrP1 and OCILrP2. Hence the genotyping of the *ocil*$^{-/-}$ mice involved RT-PCR analysis using specific oligonucleotide pairs that distinguish between OCIL and its OCILrP1 and OCILrP2 mRNA transcripts. Amplification of cDNA using the OCILm111-OCILm81 oligonucleotide pair, which detects OCIL but not OCILrP1/2, yielded a band of 426 bp in the WT mouse samples and a smaller band of 247 bp in the *ocil*$^{-/-}$ mouse samples, the latter band because of exon 3 deletion in the *ocil*$^{-/-}$ mice. Verification of the PCR-generated OCIL product was performed by Southern transfer, and detection of the hybridized product was carried out using an internal oligonucleotide probe OCILm115 (Fig. 1*B*). Because the oligonucleotide probe OCILm115 is located within exon 3, only the 426-bp amplified product in the WT samples was hybridized, whereas no hybridized product was detected in the *ocil*$^{-/-}$ samples, thus confirming successful removal of exon 3 sequence of *ocil* (Fig. 1*B*).

Oligonucleotides (OCILm113 and OCILm81) specific for the OCILrP2 amplified a product of 303 bp in WT and *ocil*$^{-/-}$ samples (Fig. 1*B*). OCILrP2 mRNA levels were unaltered in response to ablation of OCIL. In addition, we were unable to detect OCILrP1 mRNA (using OCILm114 and OCILm81) in WT or *ocil*$^{-/-}$ samples, consistent with our previous reports (2) that OCILrP1 transcripts are not expressed in osteoblasts.

Phenotypic Analysis of Ocil$^{-/-}$ Mice—ocil-deficient mice were born with expected Mendelian frequency from intercrosses of *ocil* heterozygous mice and appeared grossly normal and healthy. Both male and female *ocil* homozygous null mice were fertile and were maintained as a homozygous line, which was used for all histological and cellular experiments described below. Age- and sex-matched C57BL/6 mice from the same source were used as wild type controls.

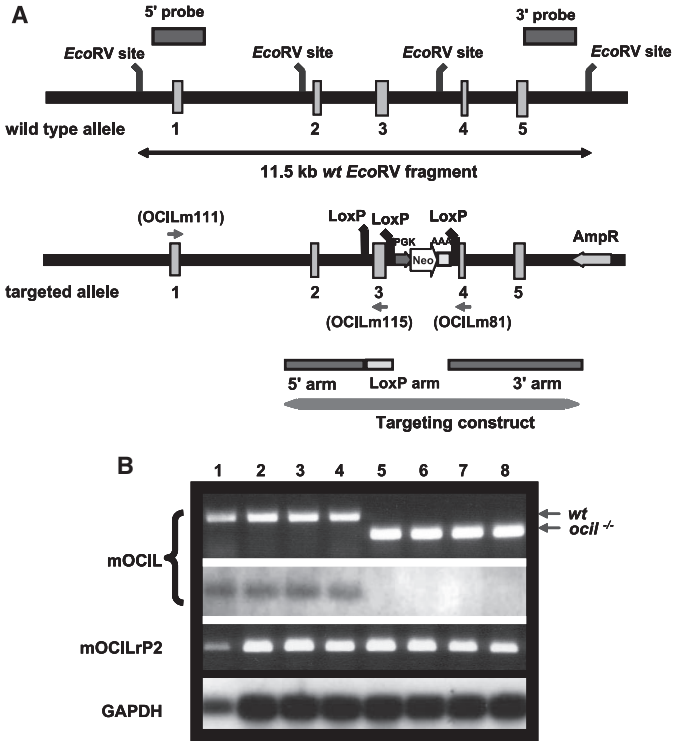

FIGURE 1. **Targeted disruption of *ocil*.** *A,* schematic representation of the targeting construct showing the wild type allele at the *top* and the targeted allele at the *bottom*. Exons 1–5 of *ocil* are depicted as *rectangles*. The targeting construct containing a PGK gene cassette and a neomycin (*Neo*) resistance gene cassette is depicted. The neo cassette and exon 3 are both flanked by LoxP sites. Construction of the *ocil*$^{-/-}$ targeting vector involved the excision of exon 3 of the *ocil* gene. Because of deletion of this exon, any read-through transcript of *ocil* that may arise because of splicing of exons 2–4 or exons 2–5 result in the introduction of a frameshift, and therefore a nonfunctional transcript of *ocil* and a resultant inactive protein. *B,* Southern blot analysis of offsprings (cDNA was reverse-transcribed from tail RNA) demonstrating successful targeting of exon 3 deletion of the *ocil* gene in *lanes 5–8* (representing 2 male and 2 female *ocil*$^{-/-}$ mice) compared with *lanes 1–4,* which represent equivalent age- and sex-matched WT controls. OCIL-specific oligonucleotides (depicted as *forward* and reverse *arrows* on the targeted allele schematic in *A*) used the following: OCILm111 (exon 1, sense) with OCILm81 (exon 4, antisense) and OCILm115 (exon 3, antisense) as the DIG-labeled detection probe. OCILrP2-specific primers used the following: OCILm113 (sense) with OCILm81 (antisense). The amount of GAPDH mRNA was used as a loading and transfer control with the following primers: GAPDH-4 (sense) with GAPDH-5 (antisense) and GAPDH-1 as the DIG-labeled detection probe.

Gross histological examination of the major organs such as liver, lung, heart, brain, thymus, spleen, intestines, skin, and skeletal muscle revealed no major abnormalities in 1-day old or 6- or 16-week-old *ocil*$^{-/-}$ mice. Loss of *ocil* did not affect the cellularity of thymus, spleen, lymph node, liver, or bone marrow (data not shown), and flow cytometry demonstrated that the percentages of cells in each tissue that expressed B cell markers (B220, IgM, and CD19), T cell and NKT cell markers (TCR$\alpha\beta$, CD4, CD8, and NK1.1), and dendritic cell and myeloid lineage markers (CD11c, CD11b, CD45RA, CD8α, Ly6G, and F4/80) were unchanged (data not shown). Dendritic cell subsets were also normally represented with no difference in base-line activation marker expression in *ocil*$^{-/-}$ mice. Because OCIL binds NK cell receptors (4), we investigated further the NK cell subsets of the *ocil*$^{-/-}$ mice; however, normal levels of expression of the inhibitory receptors Ly49 and NKG2 were observed (data not shown).

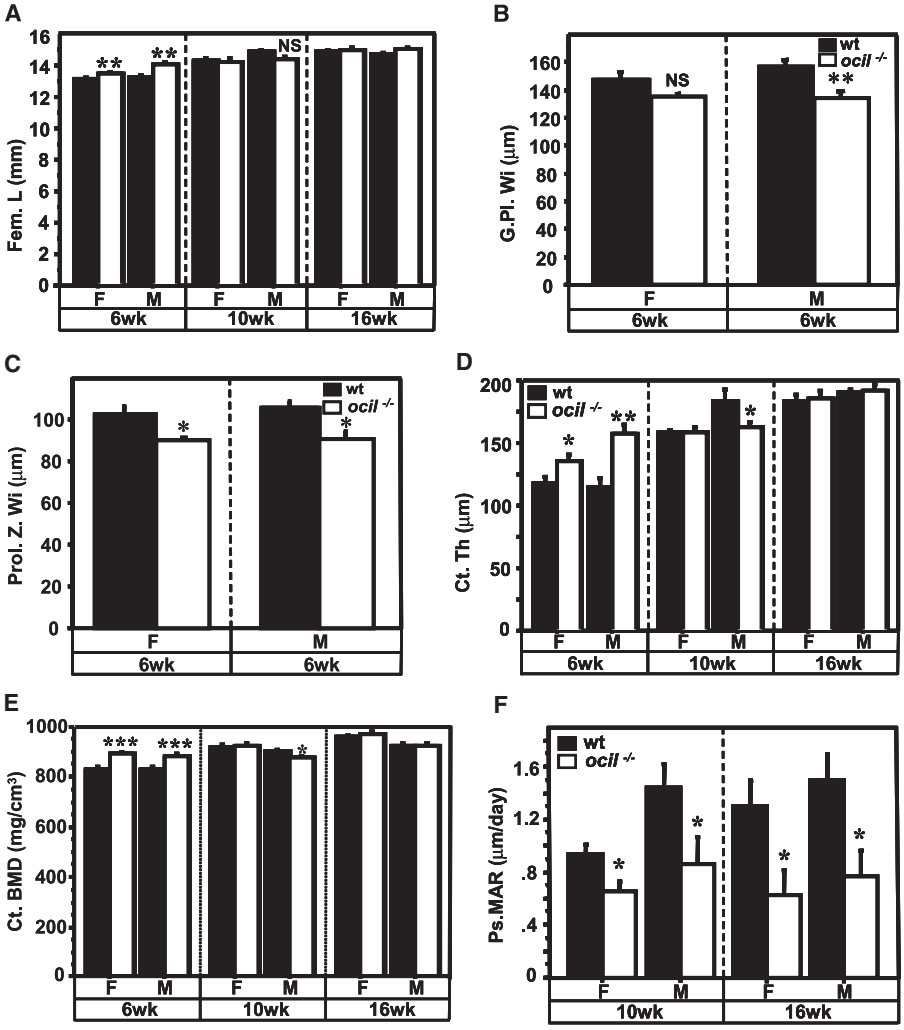

FIGURE 2. pQCT analysis of *ocil*$^{-/-}$ and WT femora (*A–E*). *A,* femoral length (*Fem.L*) in 6-, 10-, and 16-week-old mice. *B,* growth plate width (*G.Pl.Wi.*) in 6-week-old femora. *C,* proliferative zone width (*Prol.Z.Wi.*) in 6-week-old femora. *D,* cortical thickness (*Ct.Th*) in 6-, 10-, and 16-week-old femora. *E,* cortical bone mineral density (*Ct.BMD*) in 6-, 10-, and 16-week-old femora. *F,* tibial periosteal mineral appositional rate (*Ps.MAR*) in 10- and 16-week-old mice. Data are means ± S.E. on seven mice per group. *, $p < 0.05$, **, $p < 0.01$, ***, $p < 0.001$. *NS,* nonsignificant. $p = 0.07$. *F*, female; *M*, male; *wt*, wild type.

To determine whether OCIL is required for normal bone remodeling, we assessed trabecular bone parameters in the tibia. Von Kossa staining and histomorphometry revealed a significantly lower tibial trabecular bone volume in 10- and 16-week-old male *ocil*$^{-/-}$ mice compared with WT controls (Fig. 3, *A* and *B*). Other parameters measured by bone histomorphometry demonstrated a lower trabecular thickness in the 10-week-old male *ocil*$^{-/-}$ mice (Fig. 3*C*) and a decreased trabecular number in the 10- and 16-week-old male *ocil*$^{-/-}$ mice compared with WT (Fig. 3*D*). These differences indicate a mild osteopenic bone phenotype in the absence of OCIL.

The low trabecular bone volume observed in mature *ocil*$^{-/-}$ mice relative to WT control could be either caused by a reduction in bone formation or an increase in bone resorption or a combination of both. To identify the mechanism of the mild osteopenic phenotype, further histomorphometric analyses were performed. Examination of bone resorption parameters indicated an increase in the number of osteoclasts per unit bone perimeter (Fig. 4*A*), as well as an increase in osteoclast surface (data not shown) in 10-week-old male and 16-week-old female *ocil*$^{-/-}$ mice. This increase in osteoclast surface could also be observed by an increase in the number of TRAP-stained osteoclasts at the growth plate region and lining trabecular bone surfaces in representative tibial sections of 16-week-old *ocil*$^{-/-}$ female mice (Fig. 4*B*). When compared with WT mice, *ocil*$^{-/-}$ mice showed reduced bone formation rate (BFR) in the 10-week-old females and 16-week-old males (Fig. 4*C*) associated with a 54% reduction in mineralizing surface in 10-week-old females (data not shown) and a 33% reduction in mineral apposition rate in the 16-week-old males (data not shown).

In contrast to the reduced bone formation rate seen in *ocil*$^{-/-}$ mice, static markers of bone formation such as osteoblast number per bone perimeter (Fig. 4*D*), osteoblast surface, osteoid volume, osteoid surface, and osteoid thickness (data not shown) showed no significant changes in male or female *ocil*$^{-/-}$ mice, suggesting that the reduced bone formation relates to a reduction in osteoblast activity per cell rather than a change in osteoblast numbers. Furthermore, there was no significant change in the number of adipocytes within the tibial marrow cavity or the overall adipocyte volume between wild

Mild Osteopenia in Ocil$^{-/-}$ *Mice*—Contact x-ray image analysis of femora revealed that femoral length reached adult size earlier, being longer in both male and female 6-week-old *ocil*$^{-/-}$ mice (Fig. 2*A*). This difference in bone length was associated with reduced growth plate width (Fig. 2*B*), and in particular a smaller proliferative zone width in both male and female (Fig. 2*C*) 6-week-old *ocil*$^{-/-}$ mice. By 10 weeks this had normalized, and no differences in femoral length were detected at 10 or 16 weeks (Fig. 2*A*).

Although femoral width was not significantly different at any time, femoral cortical thickness was greater in the 6-week-old *ocil*$^{-/-}$ mice (Fig. 2*D*), and was accompanied by a significantly greater cortical bone mineral density of the femoral diaphyses (Fig. 2*E*). These differences between WT and *ocil*$^{-/-}$ mice were no longer detected by 16 weeks of age in both male and female *ocil*$^{-/-}$ mice. This may indicate early maturation of bone at 6 weeks of age, and possibly compensating for this, the periosteal mineral apposition rate was lower in both male and female *ocil*$^{-/-}$ mice at 10 and 16 weeks of age (Fig. 2*F*).

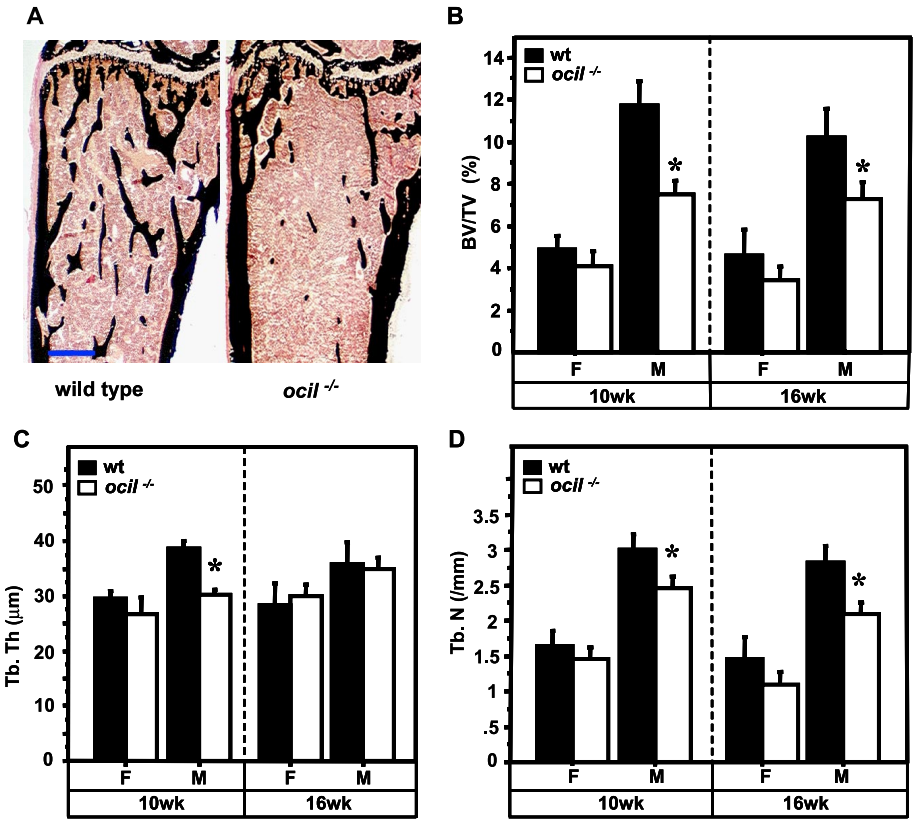

FIGURE 3. **Trabecular bone structure in *ocil*$^{-/-}$ and WT control mice.** *A,* representative sections of proximal tibiae of WT control and *ocil*$^{-/-}$ male mice at 16 weeks of age stained with modified Von Kossa stain (mineralized bone is stained *black*). *Scale bar* = 500 μm. Bone parameters (*B–D*) measured by dynamic bone histomorphometry after calcein labeling. *B,* tibial trabecular bone volume (*BV/TV*) in 6-, 10-, and 16-week-old mice; *C,* trabecular thickness (*Tb.Th*) in 10- and 16-week-old mice; and *D,* trabecular number in 10- and 16-week-old mice. Data are means ± S.E. on seven mice per group. *, $p < 0.05$. *F*, female; *M*, male; *wt*, wild type.

type and *ocil*$^{-/-}$ mice (data not shown). Thus, the mild osteopenic bone phenotype in males is attributable to higher osteoclast numbers without a concomitant coupled increase in osteoblast numbers. In females, the transient reduction in mineralizing surface (as a result of low BFR) coupled with a late increase in osteoclast formation did not give rise to any bone loss.

These data prompted us to analyze serum calcium and PTH levels of the 10- and 16-week-old *ocil*$^{-/-}$ mice. Serum calcium levels were significantly elevated in both male and female 16-week-old *ocil*$^{-/-}$ mice but were normal in the 10-week-old *ocil*$^{-/-}$ mice (Fig. 5*A*). Serum PTH levels were appropriately suppressed in the presence of elevated serum calcium in both male and female 10- and 16-week-old female *ocil*$^{-/-}$ mice (Fig. 5*B*) presumably the result of the uncoupling of bone formation and bone resorption as seen by the increased osteoclastic activity in the *ocil*$^{-/-}$ mice.

Impaired Expression of Osteoblastic Markers in Undifferentiated Primary Ocil$^{-/-}$ *Calvarial Cells*—Because BFR was decreased in 10-week-old female and 16-week-old male *ocil*$^{-/-}$ mice (Fig. 4*B*), we assessed more closely the expression levels of osteoblast-specific marker genes in undifferentiated primary calvarial cells of *ocil*$^{-/-}$ mice. *ocil*$^{-/-}$ and WT calvarial cells grown in culture for 4–5 days were cultured overnight in α-MEM with 10% FBS in the absence of ascorbate or other osteoblastogenic medium components. Cells were then harvested, and total RNA was isolated and used in quantitative real time RT-PCR assays with HPRT1 as an internal normalizing control.

Consistent with the low BFR observed in adult *Ocil*$^{-/-}$ mice, a number of osteoblast phenotypic markers, such as collagen 1-A1 (Col1-A1), alkaline phosphatase, bone sialoprotein, and osteocalcin, were expressed at considerably reduced levels in *ocil*$^{-/-}$ primary calvarial cells compared with WT (Fig. 6*A*). In contrast, PTHR1 mRNA levels (Fig. 6*A*) were unchanged. Transcription factors critical for osteoblast differentiation, such as osterix and Bril (bone restricted ifitm-like protein or interferon-inducible transmembrane protein 5 (ifitm5)/fragilis family) but not Runx2 (Fig. 6*B*) or Twist 1/2 (data not shown), were also significantly reduced. Other markers representative of a mature osteoblast phenotype such as osteopontin, IL-18, and ost-ptp (also known as Ptprv and Esp) were unchanged (data not shown). Messenger RNA levels for RANKL were elevated in *ocil*$^{-/-}$ primary calvarial cells, whereas its decoy receptor OPG was not affected (Fig. 6*B*). Combined, this phenotypic profile may suggest a preponderance of less mature osteoblastic cells.

Although there was no change in marrow adiposity *in vivo*, because osteoblasts and adipocytes share a common stromal precursor, we further assessed transcriptional factors and markers that are commonly involved in adipocyte differentiation such as PPARγ, C/EBPδ, C/EBPα, adiponectin, and resistin. *ocil*$^{-/-}$ primary osteoblasts showed a 40% reduction in C/EBPα mRNA, a 4-fold increase in adiponectin mRNA, and a 9-fold increase in resistin mRNA levels with no change in PPARγ or C/EBPδ mRNA levels (Fig. 6*C*).

Together these data provide evidence that *ocil* deficiency is also having a significant effect on the phenotypic profile of osteoblasts *in vitro* and is consistent with the reduced BFR observed in both male and female adult *ocil*$^{-/-}$ mice *in vivo*. *ocil*$^{-/-}$ mice therefore appear to have less mature osteoblasts *in vivo* and *in vitro*. However, this does not have a substantial physiological effect when compared with its actions upon osteoclast formation (further described below).

Increased Osteoclastogenesis in the Absence of Ocil—To further study the cellular mechanisms that account for the osteopenic phenotype of the *ocil*$^{-/-}$ mice, we analyzed the differentiation of osteoclasts *in vitro*. To determine whether the observed high osteoclast numbers in *ocil*$^{-/-}$ mice *in vivo*

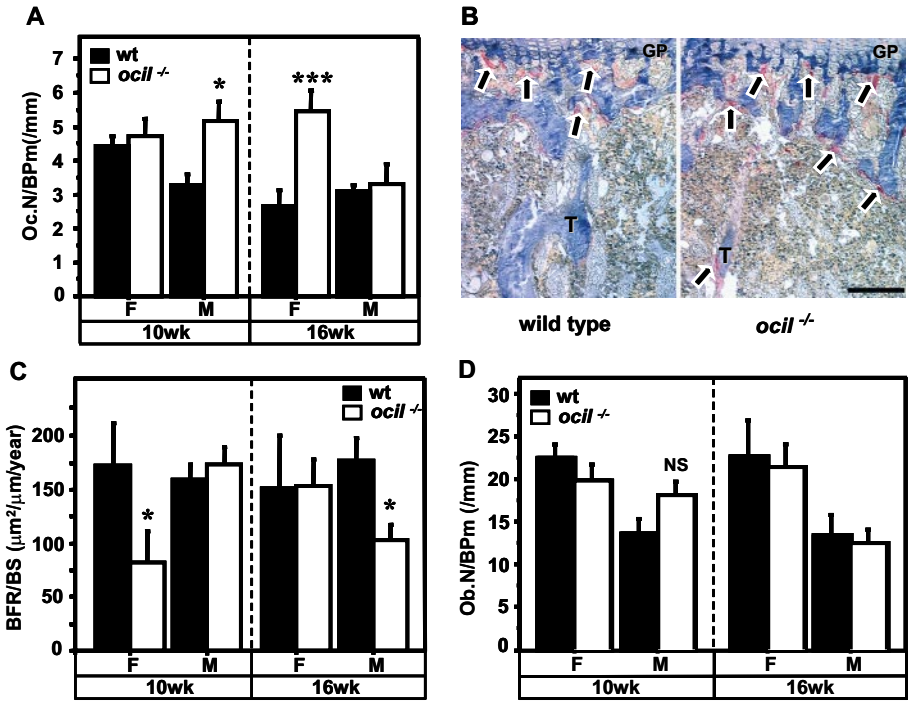

FIGURE 4. **Comparison of trabecular bone turnover in tibial sections of 10- and 16-week-old *ocil*$^{-/-}$ and WT control mice.** Bone resorption parameters (*A–C*) indicate the following. *A,* number of osteoclasts per mm of bone perimeter (*Oc.N/BPm*). *B,* positive TRAP staining (*black arrows* pointing to *maroon* color) on areas of resorption along the growth plate (*GP*) region and on osteoclast cells lining the bone trabeculae (*T*). Sections are representative of 16-week-old female tibiae. Hematoxylin (*light blue color*) is used as a counterstain. *Scale bar* represents 100 μm. *C,* bone formation rate per bone surface (*BFR/BS*). Static markers of bone formation. *D,* osteoblast number per bone perimeter (*Ob.N/BPm*). Data are expressed as means ± S.E. on seven mice per group. *, $p < 0.05$; ***, $p < 0.001$. *NS*, nonsignificant. $p = 0.07$. *F*, female; *M*, male; *wt*, wild type.

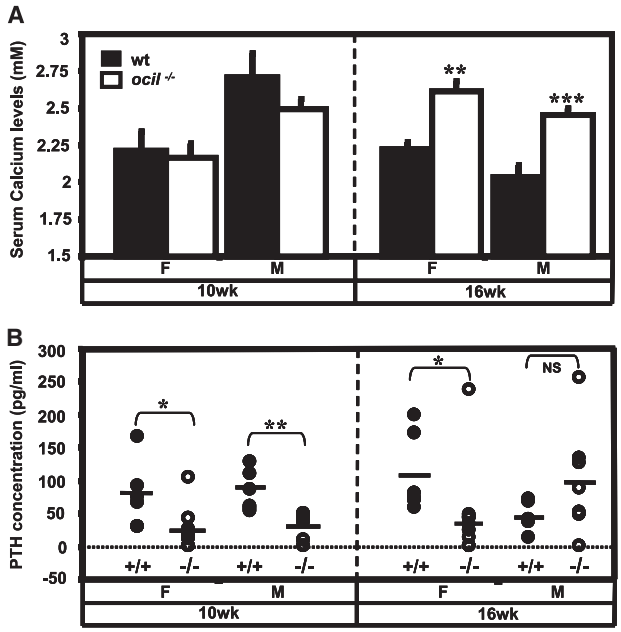

FIGURE 5. *A,* serum calcium assay. Serum calcium levels were significantly elevated in both male (*M*) and female (*F*) 16-week-old *ocil*$^{-/-}$ mice but were normal in the 10-week-old *ocil*$^{-/-}$ mice. All data are presented as means ± S.E. ($n = 6–15$ per group); **, $p < 0.01$ and ***, $p < 0.001$. *B,* univariate scattergram representing serum PTH levels in *ocil*$^{-/-}$ *versus* WT (wild type) control mice. Serum PTH levels were significantly lower in both male and female10-week-old *ocil*$^{-/-}$ mice and in 16-week-old female *ocil*$^{-/-}$ mice. Mean values are represented by *horizontal stroke lines* (——) ($n = 6–10$ per group). *NS*, nonsignificant. *, $p < 0.05$; **, $p < 0.01$.

was intrinsic to the osteoclast precursors and/or to the osteoblastic stimulation, we performed *in vitro* co-culture experiments whereby the generation of functional osteoclasts from hematopoietic precursors (bone marrow cells) is dependent on 1,25-vitamin D_3-stimulated stromal cells or osteoblasts. Osteoclast formation was greater in co-cultures containing *ocil*$^{-/-}$ bone marrow than WT, regardless of the genotype of the osteoblasts (Fig. 7*A*). This was also noted in co-cultures employing KUSA-O stromal cells (Fig. 7*B*), suggesting that differences in osteoclast numbers were dependent upon OCIL production within the bone marrow. Consistent with this, when osteoclasts were formed using bone marrow cells stimulated by recombinant M-CSF and RANKL (*i.e.* in the absence of stromal cells), the differentiation of *ocil*$^{-/-}$ precursors into TRAP-positive multinucleated osteoclasts was 50% greater than that of WT control cells (Fig. 7*C*). This was also observed when spleen cells from *ocil*$^{-/-}$ mice were used as the source of osteoclast precursors instead of bone marrow (Fig. 7*D*), indicating the production of OCIL by hematopoietic cells was crucial for limiting osteoclast formation.

DISCUSSION

It is becoming well recognized that there is interdependence between the immune system and bone physiology (23, 24). Notably, several of the key regulatory molecules that affect the action of bone formation or bone resorption also impact upon immune cell differentiation or function. Such examples include RANKL, which is critical for osteoclast differentiation as well as for lymph node genesis (25). Several cytokines and growth factors (*e.g.* IL-4, IL-10, IL-11, IL-13, IL-17, IL-18, and estrogen) have actions upon osteoclast differentiation and lymphocyte development or in some cases act through the lymphocyte to impart actions upon osteoclast formation (26, 27). The osteoclast inhibitory lectin (OCIL), a member of the NK cell C-type lectins, adds to the repertoire of factors that combine immune cell functions with actions on bone cells.

NK cell C-type lectins have a described role in autoimmune cell function, and we have previously described their emerging role to regulate osteoblast formation from mesenchyme-derived stromal cells and osteoclast formation or activity. This work extends our previous observations, and we provide herein the first demonstration for a significant role for an NK cell C-type lectin in bone metabolism *in vivo*. Loss of

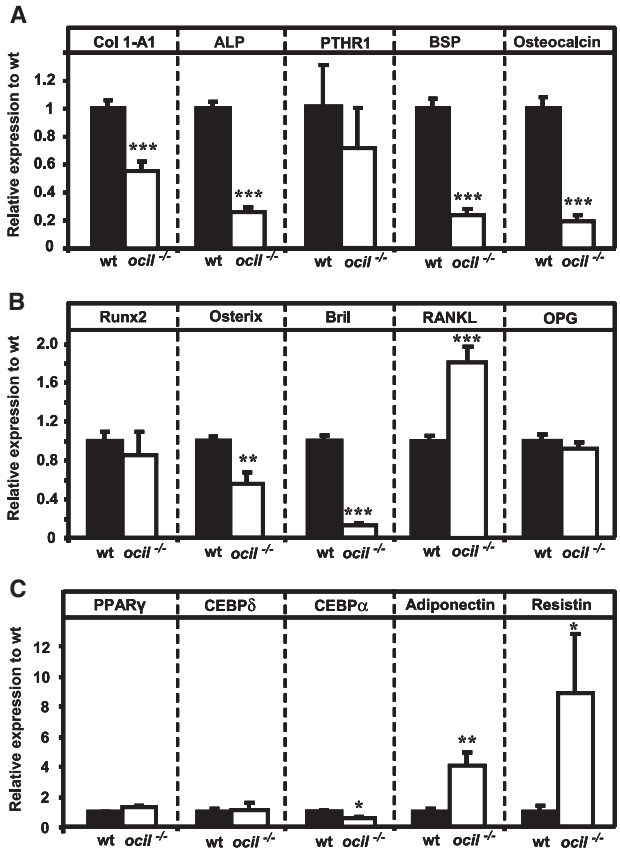

FIGURE 6. **Real time PCR analysis of mRNAs for various osteoblast-specific markers of differentiation and/or transcription factors (*A* and *B*) as well as mRNAs for gene markers commonly involved in adipocyte differentiation (*C*) in nondifferentiated *ocil*$^{-/-}$ and WT calvarial cells.** Examples shown are pooled data from two independent RNA experiments. The relative expression levels were normalized for HPRT1 expression. Relative mRNA levels in *ocil*$^{-/-}$ samples were normalized against WT control mRNA levels. *PTHR1,* parathyroid hormone receptor 1; *BSP,* bone sialoprotein; *Bril,* bone restricted ifitm-like protein; *OPG*, osteoprotegerin; *C/EBPδ,* CCAAT-enhancing binding protein δ; *C/EBPα,* CCAAT-enhancing binding protein α. *Error bars* represent S.E. *, $p < 0.05$; **, $p < 0.01$; ***, $p < 0.001$; *wt*, wild type.

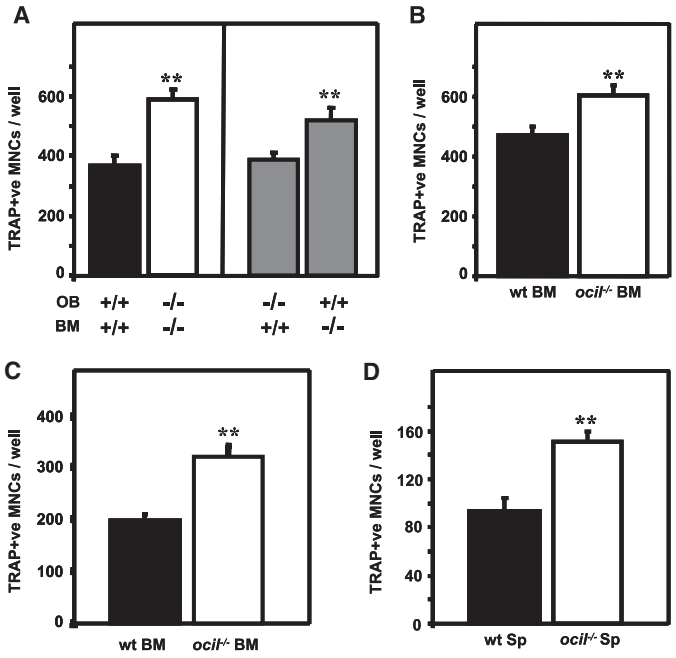

FIGURE 7. **Increased osteoclastogenesis in the absence of *ocil*.** *A,* numbers of TRAP +ve multinucleated cells per 100,000 bone marrow (*BM*) cells (from WT or *ocil*$^{-/-}$ mice) co-cultured with 20,000 primary calvarial cells (from WT or *ocil*$^{-/-}$ mice) in the presence of 1,25$(OH)_2D_3$ (10 nM) and prostaglandin E_2 (100 nM) for 7 days. *OB*, osteoblast. *Black bar* represents WT co-cultures; *white bar* represents *ocil*$^{-/-}$ co-cultures; *gray bars* represent crossover co-cultures. *B,* numbers of TRAP +ve MNCs per 100,000 bone marrow (*BM*) cells (from WT or *ocil*$^{-/-}$ mice) co-cultured with 20,000 KUSA-O stromal cells in the presence of 1,25$(OH)_2D_3$ (10 nM) and prostaglandin E_2 (100 nM) for 7 days. *C,* numbers of TRAP +ve multinucleated cells per 100,000 bone marrow (*BM*) cells (from WT or *ocil*$^{-/-}$ mice) cultured in the presence of RANKL (100 ng/ml) and M-CSF (25 ng/ml) for 7 days. *D,* numbers of TRAP +ve MNCs per 100,000 spleen (*Sp*) cells (from WT or *ocil*$^{-/-}$ mice) cultured in the presence of RANKL (50 ng/ml) and M-CSF (25 ng/ml) for 7 days. *MNC* indicates multinucleated cells (*i.e.* two or more nuclei). Data are represented as the mean ± S.E. ($n = 3$). **, $p < 0.01$; *wt*, wild type (unpaired Student's *t* test).

the NK cell C-type lectin (OCIL also known as clrb) resulted in osteopenia in adult mice as a result of increased osteoclastogenesis and decreased bone formation. Enhanced osteoclast formation was apparent when either bone marrow or splenic cultures from *ocil*$^{-/-}$ mice were cultured *in vitro* relative to cultures established from WT animals; increased osteoclast numbers were also detected transiently *in vivo*. The enhanced osteoclastic activity (partly as a result of the increased recruitment of osteoclasts) led to elevated serum calcium levels in 16-week-old *ocil*$^{-/-}$ mice compared with WT control mice. Because calcium metabolism is controlled in large part through the actions of PTH and other hormones and/or growth factors produced by bone cells or endocrine tissues, the resultant suppression of circulating PTH in the 10-week-old *ocil*$^{-/-}$ mice may indicate that these levels were suppressed to maintain normal calcium homeostasis.

The *ocil*$^{-/-}$ mice appeared healthy and were fertile, and phenotypic abnormalities were limited to bone. Given the importance of Nkrp1d (a protein ligand of OCIL), some immune system abnormalities might be anticipated, however, all blood parameters examined and circulating B and T cell populations were normal. Any specific immune defects may not be readily observed during normal physiology and may require an animal to be immunologically challenged for these to be revealed.

Loss of OCIL was associated with earlier maturation of long bones (femora) in 6-week-old *ocil*$^{-/-}$ mice, which was associated with a decreased growth plate proliferative zone width: the mechanism causing this change in bone size or whether the altered proliferative zone width is the cause or effect of this change is still not clear. These changes revert to normal by 10 and 16 weeks of age in *ocil*$^{-/-}$ mice, suggesting that this effect is transient and does not have a profound growth effect in adult mice.

What was apparent in 10-week and 16-week-old *ocil*$^{-/-}$ mice was a reduction in trabecular bone volume and trabecular number together with reduced levels of bone formation rate (both in trabecular and cortical bone), resulting in an osteopenic phenotype. The low trabecular bone volume is explained by the greater osteoclast surface and number observed in the 10-week-old *ocil*$^{-/-}$ male mice. It is well known that osteoblast and osteoclast actions *in vivo* are closely coupled such that inhibitors that suppress osteoclast formation or survival also tend to affect osteoblast activation

and osteogenesis. It was therefore somewhat surprising that removal of an osteoclast inhibitor such as OCIL did not result in a coupled increase in osteogenesis *in vivo*, in fact a decrease in bone formation was evident. However, as OCIL is one of a family of structurally related C-type lectins that includes at least four other members that appear to be evolutionarily related and have arisen by gene duplication (1), degeneracy in physiological action between these other members and as yet other undiscovered C-type lectins cannot be excluded. Further analyses of bone marrow/osteoblast co-culture assays determined that the higher osteoclast numbers observed in *ocil*$^{-/-}$ mice *in vivo* was intrinsic to the osteoclast precursor population and not a result of any cellular communication derived from the osteoblasts.

Recently, a polymorphism in OCIL has been associated with an age-dependent reduction in bone mineral density in postmenopausal women (28). Although the significance of the N19K substitution for human OCIL upon its biological activity is not known, it is clearly associated with a bone mass phenotype. Moreover, the age-dependent relationship of this polymorphism in humans is reminiscent of the bone phenotype of the *ocil*$^{-/-}$ mice we describe here.

Although the actions of OCIL were predominantly upon osteoclast differentiation and progenitor populations both *in vivo* and *ex vivo*, we nevertheless assessed osteoblast numbers and functions *in vivo* and *ex vivo*. Assessment of mRNA expression levels of various osteoblast-specific marker genes in undifferentiated primary calvarial *ocil*$^{-/-}$ cells *in vitro* (*ex vivo*), revealed a significantly altered phenotypic profile of these cells with respect to similarly derived calvarial cells from WT mice. Osteoblast phenotypic markers such as Col1-A1, alkaline phosphatase, bone sialoprotein, and osteocalcin, including the transcription factor osterix, and Bril, were all significantly reduced in *ocil*$^{-/-}$ calvarial cells compared with WT controls. This is consistent with the low trabecular BFR observed in adult *ocil*$^{-/-}$ mice *in vivo* and the reduced periosteal mineral apposition rate in both male and female *ocil*$^{-/-}$ mice at 10 and 16 weeks of age.

In addition to the less mature osteoblastic phenotype observed in *ocil*$^{-/-}$ calvarial cells *in vitro*, these cells also produce higher RANKL levels than wild type cells. This is consistent with previous data suggesting that less differentiated osteoblasts express higher levels of RANKL than mature osteoblasts (26). Therefore, the enhanced osteoclast formation in *ocil*$^{-/-}$ mice may result from a contribution of both elevated RANKL levels and the removal of the natural osteoclast inhibitory action of OCIL. The latter appears to predominate in *in vitro* assays because deletion of OCIL from osteoclast progenitors was the only mechanism that allowed enhanced osteoclast formation (Fig. 7). Furthermore, certain markers involved in adipocyte differentiation (*e.g.* adiponectin and resistin) were also significantly altered in these cells. This is not surprising because osteoblasts and adipocytes share a common stromal precursor, and we have demonstrated that recombinant OCIL (expressed as a soluble protein) inhibits both osteoblast and adipocyte differentiation, but not myocyte differentiation of mesenchyme-derived stromal cells (29).

We targeted the deletion of OCIL because it was the prototype of a family of related molecules, and the most robustly regulated family member by calcitropic hormones and growth factors (1). It is possible that degeneracy exists *in vivo* in the functions of OCIL, OCILrP2, and similar C-type lectins to OCIL; however, clarification of this point awaits further targeted deletions of these other family members. Collectively, our data suggest that OCIL is a key negative regulator of osteoclastogenesis, and loss of OCIL resulted in mild osteopenia, which was accompanied by greater numbers of osteoclast precursors in both bone marrow and other hematopoietic organs such as the spleen. Thus, OCIL provides another link between immune cell function and bone physiology.

REFERENCES

1. Zhou, H., Kartsogiannis, V., Hu, Y. S., Elliott, J., Quinn, J. M., McKinstry, W. J., Gillespie, M. T., and Ng, K. W. (2001) *J. Biol. Chem.* **276,** 14916–14923
2. Zhou, H., Kartsogiannis, V., Quinn, J. M., Ly, C., Gange, C., Elliott, J., Ng, K. W., and Gillespie, M. T. (2002) *J. Biol. Chem.* **277,** 48808–48815
3. Hu, Y. S., Zhou, H., Myers, D. E., Quinn, J. M. W., Atkins, G. J., Ly, C., Gange, C., Kartsogiannis, V., Elliott, J., Kostakis, P., Zannettino, A. C. W., Cromer, B., McKinstry, W. J., Findlay, D. M., Gillespie, M. T., and Ng, K. W. (2004) *J. Bone Miner. Res.* **19,** 89–99
4. Iizuka, K., Naidenko, O. V., Plougastel, B. F., Fremont, D. H., and Yokoyama, W. M. (2003) *Nat. Immunol.* **4,** 801–807
5. Katsu, Y., Lubahn, D. B., and Iguchi, T. (2003) *Endocrinology* **144,** 2597–2605
6. Gange, C. T., Quinn, J. M., Zhou, H., Kartsogiannis, V., Gillespie, M. T., and Ng, K. W. (2004) *J. Biol. Chem.* **279,** 29043–29049
7. Carlyle, J. R., Jamieson, A. M., Gasser, S., Clingan, C. S., Arase, H., and Raulet, D. H. (2004) *Proc. Natl. Acad. Sci. U. S. A.* **101,** 3527–3532
8. Plougastel, B., Dubbelde, C., and Yokoyama, W. M. (2001) *Immunogenetics* **53,** 209–214
9. Yokoyama, W. M., and Plougastel, B. F. (2003) *Nat. Rev. Immunol.* **3,** 304–316
10. Tian, W., Nunez, R., Cheng, S., Ding, Y., Tumang, J., Lyddane, C., Roman, C., and Liou, H. C. (2005) *Cell. Immunol.* **234,** 39–53
11. Umezawa, A., Maruyama, T., Segawa, K., Shadduck, R. K., Waheed, A., and Hata, J. (1992) *J. Cell. Physiol.* **151,** 197–205
12. Allan, E. H., Ho, P. W., Umezawa, A., Hata, J., Makishima, F., Gillespie, M. T., and Martin, T. J. (2003) *J. Cell. Biochem.* **90,** 158–169
13. Kontgen, F., Suss, G., Stewart, C., Steinmetz, M., and Bluethmann, H. (1993) *Int. Immunol.* **5,** 957–964
14. Leary, N. O., Pembroke, A., and Duggan, P. F. (1992) *Clin. Chem.* **38,** 904–908
15. Vremec, D., Zorbas, M., Scollay, R., Saunders, D. J., Ardavin, C. F., Wu, L., and Shortman, K. (1992) *J. Exp. Med.* **176,** 47–58
16. Sims, N. A., Brennan, K., Spaliviero, J., Handelsman, D. J., and Seibel, M. J. (2006) *Am. J. Physiol.* **290,** E456–E462
17. Parkinson, I. H., Fazzalari, N. L., Durbridge, T. C., and Moore, R. J. (1991) *J. Histotechnol.* **14,** 81–83
18. Parfitt, A. M., Drezner, M. K., Glorieux, F. H., Kanis, J. A., Malluche, H., Meunier, P. J., Ott, S. M., and Recker, R. R. (1987) *J. Bone Miner. Res.* **2,** 595–610
19. Sims, N. A., Dupont, S., Krust, A., Clement-Lacroix, P., Minet, D., Resche-Rigon, M., Gaillard-Kelly, M., and Baron, R. (2002) *Bone* (*Elmsford*) **30,** 18–25
20. Schmidt, C., Priemel, M., Kohler, T., Weusten, A., Muller, R., Amling, M., and Eckstein, F. (2003) *J. Bone Miner. Res.* **18,** 1486–1496
21. Horwood, N. J., Udagawa, N., Elliott, J., Grail, D., Okamura, H., Kurimoto, M., Dunn, A. R., Martin, T., and Gillespie, M. T. (1998) *J. Clin. Investig.* **101,** 595–603
22. Horwood, N. J., Elliott, J., Martin, T. J., and Gillespie, M. T. (2001) *J. Im-*

munol. **166,** 4915–4921
23. Walsh, M. C., Kim, N., Kadono, Y., Rho, J., Lee, S. Y., Lorenzo, J., and Choi, Y. (2006) *Annu. Rev. Immunol.* **24,** 33–63
24. Takayanagi, H. (2007) *Nat. Rev. Immunol.* **7,** 292–304
25. Kim, D., Mebius, R. E., MacMicking, J. D., Jung, S., Cupedo, T., Castellanos, Y., Rho, J., Wong, B. R., Josien, R., Kim, N., Rennert, P. D., and Choi, Y. (2000) *J. Exp. Med.* **192,** 1467–1478
26. Quinn, J. M., and Gillespie, M. T. (2005) *Biochem. Biophys. Res. Commun.* **328,** 739–745
27. Gillespie, M. T. (2007) *Arthritis Res. Ther.* **9,** 103
28. Pineda, B., Laporta, P., Cano, A., and Garcia-Perez, M. A. (2008) *Calcif. Tissue Int.* **82,** 348–353
29. Nakamura, A., Ly, C., Cipetic, M., Sims, N. A., Vieusseux, J., Kartsogiannis, V., Bouralexis, S., Saleh, H., Zhou, H., Price, J. T., Martin, T. J., Ng, K. W., Gillespie, M. T., and Quinn, J. M. (2007) *Bone* (*Elmsford*) **40,** 305–315